10.1098/rspa.2003.1174

THE ROYAL SOCIETY

Eshelby problem of polygonal inclusions in anisotropic piezoelectric bimaterials

By E. Pan

Department of Civil Engineering, The University of Akron, Akron, OH 44325-3905, USA (pan2@uakron.edu)

Received 3 February 2003; revised 9 April 2003; accepted 23 April 2003; published online 4 December 2003

This paper studies the two-dimensional Eshelby problem in anisotropic piezoelectric bimaterials. Assuming that the inclusion is an arbitrarily shaped polygon with uniform eigenstrain and eigenelectric fields, we derive the exact closed-form solution by integrating analytically the line-source Green functions in the corresponding bimaterials. The required line-source Green functions are obtained in terms of the Stroh formalism and include six different interface models. Since the induced elastic and piezoelectric fields due to the eigenstrain and eigenelectric fields are given in the exact closed form in terms of simple elementary functions, those due to multiple inclusions can be superposed together. Benchmark numerical examples are also presented for the induced elastic and piezoelectric fields within a square inclusion due to a uniform hydrostatic eigenstrain with the bimaterials being made of typical quartz and ceramic.

Keywords: Eshelby problem; Green's function; anisotropic piezoelectric bimaterials; Stroh formalism; imperfect interface; quantum wires

1. Introduction

It is well known that the Eshelby problem (Eshelby 1957, 1959, 1961; Willis 1981; Mura 1987; Dunn & Taya 1993) is fundamental to various engineering and physical fields, and thus is the subject of continuing studies (Bacon *et al.* 1978; Mura 1987; Ting 1996; Buryachenko 2001). In recent years, the Eshelby problem of any shaped inclusion has been found to be particularly useful in the study of nanoscale semiconductor quantum devices (Gosling & Willis 1995; Faux & Pearson 2000; Glas 2001). The embedded quantum dot (QD) and quantum wire (QWR) can induce large elastic and piezoelectric fields which in turn can have a strong influence on the electronic and optical properties of the semiconductor nanostructures (see, for example, Singh 1993; Davies 1998*a*, *b*; Bimberg *et al.* 1999; Ram-Mohan 2002; Freund & Johnson 2001; Waltereit *et al.* 2002). It is further noted that piezoelectric coupling could be an important contribution to the electronic and optical properties of the semiconductor structure, due to the fact that most semiconductor materials are piezoelectric (Davies & Larkin 1994; Jogai 2001; Pan 2002*a*, *b*; Pan & Yang 2003).

In the study of the Eshelby problem, material anisotropy poses great difficulty. While, for the three-dimensional (3D) case, Yu *et al.* (1994) derived the solution for inclusions in a transversely isotropic and elastic bimaterial space, Ru (2000,

2001) proposed a conformal mapping solution for an arbitrarily shaped inclusion in an anisotropic piezoelectric full plane, half-plane, or bimaterial full plane, under the assumption of two-dimensional (2D) deformation. For the purely elastic cubic bimaterial full plane, on the other hand, Yu (2001) obtained exact closed-form solutions for the Eshelby problem. More recently, the author derived an exact closed-form solution for an arbitrarily shaped polygonal inclusion in an anisotropic piezoelectric full plane and half-plane (Pan 2004). Until now, however, an exact closed-form solution of the Eshelby problem in the corresponding anisotropic piezoelectric bimaterial full plane has still been unavailable in the literature. Yet, such a solution, if obtained in an exact closed form, is very desirable in current nanoscale QWR structure analysis as well as in various engineering and physical fields. Furthermore, the exact closed-form solution to the Eshelby problem can serve directly as the kernel function in various boundary-integral-equation formulations.

In this paper, we thus present the exact closed-form solution for an arbitrarily shaped polygonal inclusion in anisotropic piezoelectric bimaterials. We first express the induced elastic and piezoelectric fields in terms of a line integral on the boundary of the inclusion, based on the equivalent body-force concept of eigenstrain and eigenelectric fields. In the line-integral expression, the integrand is the line-source Green functions of the bimaterials, which have been also derived in this paper for six different interface models. We then carry out the line integral analytically assuming that the inclusion is a polygon. The most striking feature is that the final exact closed-form solution involves only elementary functions. Consequently, the elastic and piezoelectric fields due to multiple inclusions or an array of QWRs can be obtained easily by the superposition method. Furthermore, the induced field due to an elliptical inclusion can also be obtained by approximating the curvilinear element on the boundary of the inclusion with the straight-line element. Numerical results are presented as benchmarks where the inclusion is a square-shaped QWR under a hydrostatic eigenstrain, with the bimaterials being made of typical quartz and ceramic. We further remark that the present exact closed-form solution for the Eshelby problem in anisotropic piezoelectric bimaterials also includes the Eshelby solution corresponding to the anisotropic elastic bimaterials as a special case, for which the exact closed-form solution is also unavailable.

This paper is organized as follows: In § 2, the Eshelby problem in anisotropic piezoelectric bimaterials is described using shorthand notation. In § 3, we first define the equivalent body force of the eigenstrain and eigenelectric field, and then derive the boundary integral expression for the induced elastic and piezoelectric fields in terms of the line-source Green functions. In § 4, the exact closed-form solution for the induced elastic and electric fields due to a polygonal inclusion of arbitrary shape is derived. While benchmark numerical examples are presented in § 5, certain conclusions are drawn in § 6. The six different interface models are briefly described in Appendix A, and the related bimaterial Green functions are derived in Appendix B. Finally, the exact closed-form expressions for the line integral of the bimaterial Green functions on the boundary of the inclusion are presented in Appendix C.

2. Description of the Eshelby problem in bimaterial full plane

Consider an anisotropic and piezoelectric bimaterial full-plane (x, z), where $z > 0$ and $z < 0$ are occupied by materials 1 and 2, respectively, with the interface being on the

$z = 0$ plane. Let us assume that there is an extended general eigenstrain $\gamma^*_{Ij}(\gamma^*_{ij}, -E^*_j)$ within the domain V bounded by the surface ∂V in material α ($\alpha = 1, 2$) (see figure 1 for an inclusion in material 2). Our task is to find the induced elastic and piezoelectric fields due to the inclusion.

To facilitate our discussion, let us define the extended field quantities, including the displacement, strain, stress, and stiffness matrix, as (Barnett & Lothe 1975; Dunn & Taya 1993; Pan 1999)

$$u_I = \begin{cases} u_i, & I = 1, 2, 3, \\ \phi, & I = 4, \end{cases} \tag{2.1}$$

$$\gamma_{Ij} = \begin{cases} \gamma_{ij} = 0.5(u_{j,i} + u_{i,j}), & I = 1, 2, 3, \\ -E_j = \phi_{,j}, & I = 4, \end{cases} \tag{2.2}$$

$$\sigma_{iJ} = \begin{cases} \sigma_{ij}, & J = 1, 2, 3, \\ D_i, & J = 4, \end{cases} \tag{2.3}$$

$$C_{iJKl} = \begin{cases} C_{ijkl}, & J,\ K = 1, 2, 3, \\ e_{lij}, & J = 1, 2, 3,\ K = 4, \\ e_{ikl}, & J = 4,\ K = 1, 2, 3, \\ -\varepsilon_{il}, & J = K = 4. \end{cases} \tag{2.4}$$

In equations (2.1)–(2.4), u_i and ϕ are the elastic displacement and electrical potential, respectively; γ_{ij} is the elastic strain and E_i the electrical field; C_{ijlm}, e_{ijk} and ϵ_{ij} are the elastic moduli, the piezoelectric coefficients and the dielectric constants, respectively. We remark that the decoupled state (purely elastic and purely electrical deformations) can be obtained simply by setting $e_{ijk} = 0$. Therefore, the solution presented in this paper contains the solution corresponding to the anisotropic purely elastic bimaterials as a special case.

In the following sections, we will also use the *extended displacement* for the elastic displacement and electrical potential as defined by (2.1), the *extended stress* for the stress and electrical displacement as defined by (2.3), and the *extended stiffness matrix* for all the material constants as defined by (2.4). Furthermore, we define the *extended traction vector* as

$$\boldsymbol{t} = (t_1, t_2, t_3, t_4)^{\mathrm{T}} \equiv (\sigma_{31}, \sigma_{32}, \sigma_{33}, D_3)^{\mathrm{T}}. \tag{2.5}$$

To find the induced fields, a suitable interface condition is also needed. In this paper, we solve the Eshelby problem for six different interface conditions. For the perfect-bond interface condition, we require that the extended displacement and traction vectors be continuous across the interface, i.e.

$$u^{(1)}_J|_{z=0^+} = u^{(2)}_J|_{z=0^-}, \quad t^{(1)}_J|_{z=0^+} = t^{(2)}_J|_{z=0^-}, \quad J = 1, 2, 3, 4. \tag{2.6}$$

The other five imperfect interface conditions are discussed in Appendixes A and B.

3. Equivalent body-force and integral expressions

For an extended general eigenstrain γ^*_{Ij} within the domain V bounded by the surface ∂V in material α ($\alpha = 1, 2$) (figure 1), we define the total extended strain as a sum

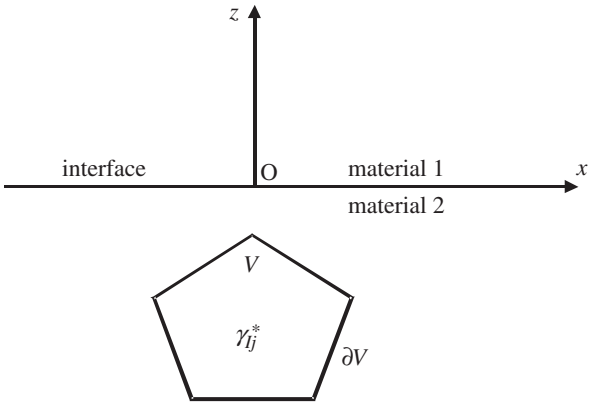

Figure 1. A general inclusion problem in an anisotropic piezoelectric bimaterial full plane: an extended eigenstrain $\gamma^*_{Ij}(\gamma^*_{ij}, -E^*_j)$ within an arbitrarily shaped polygon in material 2.

of

$$\gamma_{Ij} = \gamma^{\mathrm{e}}_{Ij} + \gamma^*_{Ij}, \tag{3.1}$$

where γ^{e}_{Ij} is the extended strain that appears in the constitutive relation, i.e.

$$\sigma_{iJ} = C_{iJKl}\gamma^{\mathrm{e}}_{Kl}, \tag{3.2}$$

or

$$\sigma_{iJ} = C_{iJKl}(\gamma_{Kl} - \chi\gamma^*_{Kl}), \tag{3.3}$$

with $\chi = 1$ if the field point is within the eigenstrain domain V and $\chi = 0$ otherwise.

Using the equilibrium equation in materials 1 and 2 for the stresses and the balance equation for the electric displacements, i.e.

$$\sigma_{iJ,i} = 0, \tag{3.4}$$

we found that, for an inclusion in material α ($\alpha = 1, 2$),

$$C^{(\alpha)}_{iJKl}u_{K,li} = C^{(\alpha)}_{iJKl}\gamma^*_{Kl,i}. \tag{3.5}$$

The right-hand side of (3.5) therefore resembles the extended body force, i.e.

$$f_J = -C^{(\alpha)}_{iJKl}\gamma^*_{Kl,i}, \tag{3.6}$$

which is the equivalent body force of eigenstrain. This equivalent body force will be employed to find the induced total extended displacement u_I and total extended strain γ_{Ij}. We further mention that the inclusion can be in material 1 ($\alpha = 1$) or in material 2 ($\alpha = 2$).

Therefore, for the eigenstrain γ^*_{Ij} at $\boldsymbol{x} = (x, z)$ within the domain V in material α, the induced extended displacement at $\boldsymbol{X} = (X, Z)$ can be found by the superposition method. That is, the response is the integral, over V, of the equivalent body force defined by (3.6) multiplied by the line-source Green functions, as

$$u_K(\boldsymbol{X}) = -\int_V u^K_J(\boldsymbol{x}; \boldsymbol{X})[C^{(\alpha)}_{iJLm}\gamma^*_{Lm}(\boldsymbol{x})]_{,i}\,\mathrm{d}V(\boldsymbol{x}), \tag{3.7}$$

where $u_J^K(\boldsymbol{x};\boldsymbol{X})$ is the Green Jth elastic displacement/electric potential at $\boldsymbol{x}$ due to a point-force/point-charge in the Kth direction applied at $\boldsymbol{X}$. Depending upon the locations of $\boldsymbol{x}$ and $\boldsymbol{X}$, this Green function has four different sets of expressions and is derived in Appendix B.

Integrating by parts and noticing that the eigenstrain is non-zero only in V, equation (3.7) can be expressed alternatively as

$$u_K(\boldsymbol{X}) = \int_V u^K_{J,x_i}(\boldsymbol{x};\boldsymbol{X}) C^{(\alpha)}_{iJLm} \gamma^*_{Lm}(\boldsymbol{x})\,\mathrm{d}V(\boldsymbol{x}). \tag{3.8}$$

If we further assume that the eigenstrain is uniform within the domain V, then the domain integral can be further transformed to the surface of V. That is

$$u_K(\boldsymbol{X}) = C^{(\alpha)}_{iJLm}\gamma^*_{Lm} \int_{\partial V} u^K_J(\boldsymbol{x};\boldsymbol{X}) n_i(\boldsymbol{x})\,\mathrm{d}S(\boldsymbol{x}), \tag{3.9}$$

where $n_i(\boldsymbol{x})$ is the outward normal on the surface of V. Again, we mention that the inclusion can be in material 1 ($\alpha = 1$) or material 2 ($\alpha = 2$).

To find the elastic strain and electric fields, we take the derivatives of equation (3.9) with respect to the field point $\boldsymbol{X}$ (i.e. the source point of the line-force/line-charge Green function), which yields (for inclusion in material α),

$$\gamma_{kp}(\boldsymbol{X}) = \tfrac{1}{2}\gamma^*_{Lm} C^{(\alpha)}_{iJLm} \int_{\partial V} [u^k_{J,X_p}(\boldsymbol{x};\boldsymbol{X}) + u^p_{J,X_k}(\boldsymbol{x};\boldsymbol{X})] n_i(\boldsymbol{x})\,\mathrm{d}S(\boldsymbol{x}), \quad k,p = 1,2,3, \tag{3.10a}$$

$$E_p(\boldsymbol{X}) = -\gamma^*_{Lm} C^{(\alpha)}_{iJLm} \int_{\partial V} u^4_{J,X_p}(\boldsymbol{x};\boldsymbol{X}) n_i(\boldsymbol{x})\,\mathrm{d}S(\boldsymbol{x}), \quad p = 1,2,3. \tag{3.10b}$$

The stresses and electric displacements are obtained from (3.3) using material properties in the corresponding domain.

We remark that the results presented are for the 2D-inclusion problem. Similar expressions can be derived for the corresponding 3D problem. We also note that the induced elastic and piezoelectric fields within the anisotropic piezoelectric bimaterials can be obtained simply by performing an integral over the surface of the inclusion, provided that the corresponding bimaterial Green functions are available. Furthermore, we will show next that, for a uniform piezoelectric eigenstrain field within an arbitrary polygon in a bimaterial full plane, the induced elastic and piezoelectric fields can be derived in the exact closed form. Such an exact closed-form solution is unavailable to the best of the author's knowledge, except for the work by Faux *et al.* (1997), where they derived the eigenstrain-induced elastic field in a purely elastic isotropic full plane analytically using a similar approach to that presented in this paper. With the bimaterial Green functions being derived in Appendix B for various interface conditions, we derive, in § 4, the exact closed-form solution for the induced field.

4. Analytical integral of an arbitrary line segment

First, we note that, in order to find the induced field due to a polygonal inclusion, one needs only to find the contribution from each straight-line segment of the boundary of the inclusion. The total induced field can be obtained by summing up the contributions from all the sides of the polygon.

Now, to carry out the line integral in equation (3.9), we first write the extended Green displacement given by equations (B 1), (B 2), (B 16) and (B 17) in Appendix B in the matrix form in the same way as we did for that in equation (3.9).

Therefore, when the source point is in material 1 ($Z > 0$), we have

$$u_J^K(\boldsymbol{x}, \boldsymbol{X}) = \frac{1}{\pi} \operatorname{Im}\{A_{JR}^{(1)} \ln(z_R^{(1)} - s_R^{(1)}) A_{KR}^{(1)}\} + \frac{1}{\pi} \operatorname{Im} \sum_{v=1}^{4} \{A_{JR}^{(1)} \ln(z_R^{(1)} - \bar{s}_v^{(1)}) Q_{RK}^{11,v}\} \tag{4.1a}$$

for the field point in material 1 ($z > 0$), and

$$u_J^K(\boldsymbol{x}, \boldsymbol{X}) = \frac{1}{\pi} \operatorname{Im} \sum_{v=1}^{4} \{A_{JR}^{(2)} \ln(z_R^{(2)} - s_v^{(1)}) Q_{RK}^{12,v}\} \tag{4.1b}$$

for the field point in material 2 ($z < 0$). In equations (4.1 *a*) and (4.2 *b*), an overbar denotes the complex conjugate, and superscripts (1) and (2) denote quantities in the material half-planes 1 and 2, respectively. Definitions for $z_R^{(\alpha)}$ and $s_v^{(\alpha)}$, and the expressions for $Q_{RN}^{11,v}$ and $Q_{RN}^{12,v}$, are given in Appendix B.

Similarly, when the source point is in material 2 ($Z < 0$), we have

$$u_J^K(\boldsymbol{x}, \boldsymbol{X}) = \frac{1}{\pi} \operatorname{Im} \sum_{v=1}^{4} \{A_{JR}^{(1)} \ln(z_R^{(1)} - s_v^{(2)}) Q_{RK}^{21,v}\} \tag{4.2a}$$

for field point in material 1 ($z > 0$), and

$$u_J^K(\boldsymbol{x}, \boldsymbol{X}) = \frac{1}{\pi} \operatorname{Im}\{A_{JR}^{(2)} \ln(z_R^{(2)} - s_R^{(2)}) A_{KR}^{(2)}\} + \frac{1}{\pi} \operatorname{Im} \sum_{v=1}^{4} \{A_{JR}^{(2)} \ln(z_R^{(2)} - \bar{s}_v^{(2)}) Q_{RK}^{22,v}\} \tag{4.2b}$$

for field point in material 2 ($z < 0$). Again, $Q_{RN}^{21,v}$ and $Q_{RN}^{22,v}$ are given in Appendix B.

Let us define a line segment in the (x, z)-plane starting from point 1 (x_1, z_1) and ending at point 2 (x_2, z_2), in terms of the parameter t $(0 \leqslant t \leqslant 1)$, as

$$\left.\begin{aligned} x &= x_1 + (x_2 - x_1)t, \\ z &= z_1 + (z_2 - z_1)t. \end{aligned}\right\} \tag{4.3}$$

Therefore, the outward normal components $n_i(\boldsymbol{x})$ are constants, given by

$$n_1 = \frac{(z_2 - z_1)}{l}, \qquad n_2 = -\frac{(x_2 - x_1)}{l}, \tag{4.4}$$

where $l = \sqrt{(x_2 - x_1)^2 + (z_2 - z_1)^2}$ is the length of the line segment. It is obvious that the elemental length is $\mathrm{d}S = l\,\mathrm{d}t$.

Note from Appendix B that, when the source and field points are in the same half-plane, the bimaterial Green functions consist of two parts: the full-plane Green function and a complementary part. However, when they are in different half-planes, the bimaterial Green functions consist only a complementary part. Consequently, the corresponding integrals can also be separated into two parts involving two types of

functions. For the integral in the full plane, i.e. the first terms in (4.1 *a*) and (4.2 *b*), we define the result, being a function of the source point $\boldsymbol{X} \equiv (X, Z)$, as

$$h_R^{(\alpha)}(X,Z) \equiv \int_0^1 \ln(z_R^{(\alpha)} - s_R^{(\alpha)})\,\mathrm{d}t. \tag{4.5}$$

Similarly, we define the integral corresponding to the complementary part as

$$g_{Rv}^{\alpha\beta}(X,Z) \equiv \int_0^1 \ln(z_R^{(\alpha)} - s_v^{(\beta)})\,\mathrm{d}t, \tag{4.6 a}$$

$$w_{Rv}^{(\alpha)}(X,Z) \equiv \int_0^1 \ln(z_R^{(\alpha)} - \bar{s}_v^{(\alpha)})\,\mathrm{d}t. \tag{4.6 b}$$

While (4.6 *a*) corresponds to the line integration of (4.1 *b*) and (4.2 *a*), expression (4.6 *b*) corresponds to the line integration of the second term in (4.1 *a*) and (4.2 *b*). The exact closed-form expressions for these integrals in (4.5) and (4.6) are given in Appendix C. Therefore, the induced elastic displacement and piezoelectric potential, due to the contribution of a straight line along the boundary, can be expressed in an exact closed form. These are given below in detail.

When the inclusion is in material 1, the induced extended displacement is

$$u_K(\boldsymbol{X}) = n_i C_{iJLm}^{(1)} \gamma_{Lm}^* \frac{l}{\pi} \operatorname{Im}\left\{ A_{JR}^{(1)} h_R^{(1)}(X,Z) A_{KR}^{(1)} + \sum_{v=1}^{4} A_{JR}^{(1)} w_{Rv}^{(1)}(X,Z) Q_{RK}^{11,v} \right\} \tag{4.7 a}$$

for the response in material 1 ($Z > 0$), and

$$u_K(\boldsymbol{X}) = n_i C_{iJLm}^{(1)} \gamma_{Lm}^* \frac{l}{\pi} \operatorname{Im}\left\{ \sum_{v=1}^{4} A_{JR}^{(1)} g_{Rv}^{12}(X,Z) Q_{RK}^{21,v} \right\} \tag{4.7 b}$$

for the response in material 2 ($Z < 0$).

Similarly, when the inclusion is in material 2, the induced extended displacement is

$$u_K(\boldsymbol{X}) = n_i C_{iJLm}^{(2)} \gamma_{Lm}^* \frac{l}{\pi} \operatorname{Im}\left\{ \sum_{v=1}^{4} A_{JR}^{(2)} g_{Rv}^{21}(X,Z) Q_{RK}^{12,v} \right\} \tag{4.7 c}$$

for the response in material 1 ($Z > 0$) and

$$u_K(\boldsymbol{X}) = n_i C_{iJLm}^{(2)} \gamma_{Lm}^* \frac{l}{\pi} \operatorname{Im}\left\{ A_{JR}^{(2)} h_R^{(2)}(X,Z) A_{KR}^{(2)} + \sum_{v=1}^{4} A_{JR}^{(2)} w_{Rv}^{(2)}(X,Z) Q_{RK}^{22,v} \right\} \tag{4.7 d}$$

for the response in material 2 ($Z < 0$).

Note that the first term is the solution corresponding to the full plane, and the second term is the contribution from the complementary part, which is used to satisfy the interface conditions of the bimaterials. Therefore, equations (4.7) give the contribution of a straight-line segment of the inclusion in the bimaterials with the inclusion being in either of the half-planes. By adding contributions from all the line segments of the boundary of the inclusion, the extended displacement solution for an inclusion with a general polygonal shape in either half-plane is then obtained in an exact closed form!

The exact closed-form strain and electric field can be obtained by simply taking the derivatives of (4.7 *a*)–(4.7 *d*) with respect to the coordinate $\boldsymbol{X} = (X, Z)$. In doing so, we obtain the elastic strain and electric field, due to a straight-line segment of the boundary of the inclusion, by the following equations (for $\alpha, \beta = 1, 3$).

When the inclusion is in material 1, we have

$$\left.\begin{aligned}
&\gamma_{\beta\alpha}(\boldsymbol{X}) \\
&\quad = 0.5 n_i C^{(1)}_{iJLm} \gamma^*_{Lm} \frac{l}{\pi} \operatorname{Im}\left\{ A^{(1)}_{JR} h^{(1)}_{R,\alpha}(X,Z) A^{(1)}_{\beta R} + \sum_{v=1}^{4} A^{(1)}_{JR} w^{(1)}_{Rv,\alpha}(X,Z) Q^{11,v}_{R\beta} \right\} \\
&\qquad + 0.5 n_i C^{(1)}_{iJLm} \gamma^*_{Lm} \frac{l}{\pi} \operatorname{Im}\left\{ A^{(1)}_{JR} h^{(1)}_{R,\beta}(X,Z) A^{(1)}_{\alpha R} + \sum_{v=1}^{4} A^{(1)}_{JR} w^{(1)}_{Rv,\beta}(X,Z) Q^{11,v}_{R\alpha} \right\}, \\
&\gamma_{2\alpha}(\boldsymbol{X}) \\
&\quad = 0.5 n_i C^{(1)}_{iJLm} \gamma^*_{Lm} \frac{l}{\pi} \operatorname{Im}\left\{ A^{(1)}_{JR} h^{(1)}_{R,\alpha}(X,Z) A^{(1)}_{2R} + \sum_{v=1}^{4} A^{(1)}_{JR} w^{(1)}_{Rv,\alpha}(X,Z) Q^{11,v}_{R2} \right\}, \\
&E_{\alpha}(\boldsymbol{X}) \\
&\quad = -n_i C^{(1)}_{iJLm} \gamma^*_{Lm} \frac{l}{\pi} \operatorname{Im}\left\{ A^{(1)}_{JR} h^{(1)}_{R,\alpha}(X,Z) A^{(1)}_{4R} + \sum_{v=1}^{4} A^{(1)}_{JR} w^{(1)}_{Rv,\alpha}(X,Z) Q^{11,v}_{R4} \right\}
\end{aligned}\right\} \tag{4.8}$$

for the response in material 1 ($Z > 0$), and

$$\gamma_{\beta\alpha}(\boldsymbol{X}) = 0.5 n_i C^{(1)}_{iJLm} \gamma^*_{Lm} \frac{l}{\pi} \operatorname{Im}\left\{ \sum_{v=1}^{4} A^{(1)}_{JR} g^{12}_{Rv,\alpha}(X,Z) Q^{21,v}_{R\beta} + \sum_{v=1}^{4} A^{(1)}_{JR} g^{12}_{Rv,\beta}(X,Z) Q^{21,v}_{R\alpha} \right\}, \tag{4.9}$$

$$\gamma_{2\alpha}(\boldsymbol{X}) = 0.5 n_i C^{(1)}_{iJLm} \gamma^*_{Lm} \frac{l}{\pi} \operatorname{Im}\left\{ \sum_{v=1}^{4} A^{(1)}_{JR} g^{12}_{Rv,\alpha}(X,Z) Q^{21,v}_{R2} \right\}, \tag{4.10}$$

$$E_{\alpha}(\boldsymbol{X}) = -n_i C^{(1)}_{iJLm} \gamma^*_{Lm} \frac{l}{\pi} \operatorname{Im}\left\{ \sum_{v=1}^{4} A^{(1)}_{JR} g^{12}_{Rv,\alpha}(X,Z) Q^{21,v}_{R4} \right\}, \tag{4.11}$$

for the response in material 2 ($Z < 0$).

Similarly, when the inclusion is in material 2, we obtain

$$\gamma_{\beta\alpha}(\boldsymbol{X}) = 0.5 n_i C^{(2)}_{iJLm} \gamma^*_{Lm} \frac{l}{\pi} \operatorname{Im}\left\{ \sum_{v=1}^{4} A^{(2)}_{JR} g^{21}_{Rv,\alpha}(X,Z) Q^{12,v}_{R\beta} + \sum_{v=1}^{4} A^{(2)}_{JR} g^{21}_{Rv,\beta}(X,Z) Q^{12,v}_{R\alpha} \right\}, \tag{4.12}$$

$$\gamma_{2\alpha}(\boldsymbol{X}) = 0.5 n_i C^{(2)}_{iJLm} \gamma^*_{Lm} \frac{l}{\pi} \operatorname{Im}\left\{ \sum_{v=1}^{4} A^{(2)}_{JR} g^{21}_{Rv,\alpha}(X,Z) Q^{12,v}_{R2} \right\}, \tag{4.13}$$

$$E_{\alpha}(\boldsymbol{X}) = -n_i C^{(2)}_{iJLm} \gamma^*_{Lm} \frac{l}{\pi} \operatorname{Im}\left\{ \sum_{v=1}^{4} A^{(2)}_{JR} g^{21}_{Rv,\alpha}(X,Z) Q^{12,v}_{R4} \right\}, \tag{4.14}$$

for the response in material 1 ($Z > 0$), and

$$\left.\begin{aligned}
&\gamma_{\beta\alpha}(\boldsymbol{X}) \\
&\quad = 0.5 n_i C^{(2)}_{iJLm} \gamma^*_{Lm} \frac{l}{\pi} \operatorname{Im}\left\{ A^{(2)}_{JR} h^{(2)}_{R,\alpha}(X,Z) A^{(2)}_{\beta R} + \sum_{v=1}^{4} A^{(2)}_{JR} w^{(2)}_{Rv,\alpha}(X,Z) Q^{22,v}_{R\beta} \right\} \\
&\qquad + 0.5 n_i C^{(2)}_{iJLm} \gamma^*_{Lm} \frac{l}{\pi} \operatorname{Im}\left\{ A^{(2)}_{JR} h^{(2)}_{R,\beta}(X,Z) A^{(2)}_{\alpha R} + \sum_{v=1}^{4} A^{(2)}_{JR} w^{(2)}_{Rv,\beta}(X,Z) Q^{22,v}_{R\alpha} \right\}, \\
&\gamma_{2\alpha}(\boldsymbol{X}) \\
&\quad = 0.5 n_i C^{(2)}_{iJLm} \gamma^*_{Lm} \frac{l}{\pi} \operatorname{Im}\left\{ A^{(2)}_{JR} h^{(2)}_{R,\alpha}(X,Z) A^{(2)}_{2R} + \sum_{v=1}^{4} A^{(2)}_{JR} w^{(2)}_{Rv,\alpha}(X,Z) Q^{22,v}_{R2} \right\}, \\
&E_{\alpha}(\boldsymbol{X}) \\
&\quad = -n_i C^{(2)}_{iJLm} \gamma^*_{Lm} \frac{l}{\pi} \operatorname{Im}\left\{ A^{(2)}_{JR} h^{(2)}_{R,\alpha}(X,Z) A^{(2)}_{4R} + \sum_{v=1}^{4} A^{(2)}_{JR} w^{(2)}_{Rv,\alpha}(X,Z) Q^{22,v}_{R4} \right\}
\end{aligned}\right\} \tag{4.15}$$

for the response in material 2 ($Z < 0$). In equations (4.8)–(4.15), the involved functions of (X, Z) are given in Appendix C.

As a generalization, equations (4.8)–(4.15) can be written as

$$\gamma_{Ij} = S_{IjLm} \gamma^*_{Lm}, \tag{4.16}$$

where S_{IjLm} is the total Eshelby tensor in the bimaterial full plane. On observation of the induced strain/electric fields (equations (4.8)–(4.15)), the total Eshelby tensor can be expressed as

$$S_{IjLm} = S^{\infty}_{IjLm} + S^{c}_{IjLm}, \tag{4.17}$$

where the first term is the Eshelby tensor in an anisotropic piezoelectric homogeneous full plane, and the second term is the one corresponding to the complementary contribution due to the material mismatch of the bimaterials.

With these strain and electric field solutions, the stresses and electric displacements are then found from equation (3.3), using the material properties corresponding to the suitable half-plane. In summary, therefore, we have derived the exact closed-form solutions for the elastic and piezoelectric fields induced by an inclusion within an arbitrary polygon in a bimaterial full plane. Since our solutions are in the exact closed form, multiple-inclusion problems can be solved simply by superposing the contributions from all the inclusions. Furthermore, a solution to the inclusion with a curved boundary can also be obtained by approximating the curvilinear element with a straight-line element.

5. Numerical examples

First, the formulation has been checked for a couple of examples. For instance, when materials 1 and 2 are identical, the inclusion solution will then reduce to the full-plane solution (Pan 2004); when one of the two material half-planes has material properties 10 orders smaller than the other, our bimaterial-inclusion solution reduces to the half-plane solution (Pan 2004). We further mention that various inclusion solutions in isotropic elasticity have been also checked carefully, including a polygonal inclusion in full- and half-planes (Rodin 1996; Faux *et al*. 1997; Glas 2002).

Having checked our bimaterial inclusion solutions, we now apply our solution to an inclusion in a real bimaterial full plane. The bimaterials are made of two typical piezoelectric materials (Pan 2002*c*): one is a left-hand quartz in a rotated coordinate system (Tiersten 1969) with elastic constants, piezoelectric coefficients and dielectric constants being, respectively,

$$[C] = \begin{bmatrix} 0.8674 & -0.0825 & 0.2715 & -0.0366 & 0 & 0 \\ -0.0825 & 1.2977 & -0.0742 & 0.057 & 0 & 0 \\ 0.2715 & -0.0742 & 1.0283 & 0.0992 & 0 & 0 \\ -0.0366 & 0.057 & 0.0992 & 0.3861 & 0 & 0 \\ 0 & 0 & 0 & 0 & 0.6881 & 0.0253 \\ 0 & 0 & 0 & 0 & 0.0253 & 0.2901 \end{bmatrix} (10^{11}\ \mathrm{N\ m^{-2}}), \tag{5.1a}$$

$$[e] = \begin{bmatrix} 0.171 & -0.152 & -0.0187 & 0.067 & 0 & 0 \\ 0 & 0 & 0 & 0 & 0.108 & -0.095 \\ 0 & 0 & 0 & 0 & -0.0761 & 0.067 \end{bmatrix} (\mathrm{C\ m^{-2}}), \tag{5.1b}$$

$$[\varepsilon] = \begin{bmatrix} 0.3921 & 0 & 0 \\ 0 & 0.3982 & 0.0086 \\ 0 & 0.0086 & 0.4042 \end{bmatrix} (10^{-10}\ \mathrm{C\ V^{-1}\ m^{-1}}). \tag{5.1c}$$

The other one is the poled lead-zirconate-titanate (PZT-4) ceramic (Dunn & Taya 1993) with elastic constants, piezoelectric coefficients and dielectric constants being, respectively,

$$[C] = \begin{bmatrix} 1.39 & 0.778 & 0.743 & 0 & 0 & 0 \\ 0.778 & 1.39 & 0.743 & 0 & 0 & 0 \\ 0.743 & 0.743 & 1.15 & 0 & 0 & 0 \\ 0 & 0 & 0 & 0.256 & 0 & 0 \\ 0 & 0 & 0 & 0 & 0.256 & 0 \\ 0 & 0 & 0 & 0 & 0 & 0.306 \end{bmatrix} (10^{11}\ \mathrm{N\ m^{-2}}), \tag{5.2a}$$

$$[e] = \begin{bmatrix} 0 & 0 & 0 & 0 & 12.7 & 0 \\ 0 & 0 & 0 & 12.7 & 0 & 0 \\ -5.2 & -5.2 & 15.1 & 0 & 0 & 0 \end{bmatrix} (\mathrm{C\ m^{-2}}), \tag{5.2b}$$

$$[\varepsilon] = \begin{bmatrix} 0.646\,05 & 0 & 0 \\ 0 & 0.646\,05 & 0 \\ 0 & 0 & 0.561\,975 \end{bmatrix} (10^{-8}\ \mathrm{C\ V\ m}). \tag{5.2c}$$

We remark that, while the quartz is a weakly coupled piezoelectric material, the ceramic is a strongly coupled one, with the degree of the electromechanical coupling, defined as

$$g = \frac{e_{\max}}{\sqrt{(\varepsilon_{\max} C_{\max})}},$$

being equal to 0.07 and 0.5 in quartz and ceramic, respectively.

Two bimaterial cases are considered. For case 1, named quartz/ceramic, material 1 (i.e. the upper half-plane with $z > 0$) is quartz and material 2 (i.e. the lower half-plane with $z < 0$) is ceramic. For case 2, named ceramic/quartz, material 1 is ceramic

and material 2 is quartz. For both cases, there is a 20 nm × 20 nm square QWR in material 2, and it is symmetrically located with respect to the z-axis, with its upper side 5 nm from the interface. The eigenstrain in the inclusion is assumed to be hydrostatic with $\gamma^*_{xx} = \gamma^*_{zz} = 0.07$, a typical magnitude in the InAs/GaAs quantum structure (Bimberg *et al.* 1999).

Figure 2*a* shows the contours of strain component γ_{xx} within the square QWR in material 2 of the quartz/ceramic, while figure 2*b* shows the same strain component for the ceramic/quartz. Note that, while the contours show certain similarities, their magnitudes are different. In particular, the magnitude of this strain component is slightly larger than the given eigenstrain (0.072 versus 0.07) when the bimaterial full plane is quartz/ceramic (figure 2*a*), and smaller than the given eigenstrain (0.054 versus 0.07) when it is ceramic/quartz (figure 2*b*).

Similarly, figure 3*a*, *b* shows the contours of hydrostatic strain $\gamma_{xx} + \gamma_{zz}$ within the square QWR in material 2 of quartz/ceramic and of ceramic/quartz, respectively. It is interesting that, for both bimaterial cases, the induced hydrostatic strain within the square QWR is roughly constant, with a value of 0.1 for the quartz/ceramic (figure 3*a*) and 0.085 for the ceramic/quartz (figure 3*b*). We remark that the same near-constant feature for the hydrostatic strain was also observed for a rectangular inclusion in an isotropic full plane (Downes *et al.* 1995).

The contour of electric component E_x (V m^{-1}) within the square QWR in material 2 of the quartz/ceramic is plotted in figure 4*a*. The corresponding result is shown in figure 4*b* for the ceramic/quartz case. We note that the induced E_x is completely different for the two bimaterial systems. Their contour shapes and magnitudes are clearly different from each other for the two bimaterial cases. In particular, the maximum magnitude in quartz/ceramic is roughly twice that in ceramic/quartz. Also, we observe that the distribution of the electric component E_x for the ceramic/quartz case (figure 4*b*) is asymmetric, due to the fact that the quartz has been rotated to become a low-symmetry monoclinic material (see equations (5.1)).

Finally, figure 5*a*, *b* shows the contours of electric component E_z (V m^{-1}) within the square QWR in material 2 of quartz/ceramic and of ceramic/quartz, respectively. Again, their magnitudes and shapes are completely different, with the maximum magnitude in quartz/ceramic being about five times larger than that in ceramic/quartz.

6. Conclusions

In this paper, we have solved the Eshelby problem of an arbitrarily shaped polygonal inclusion within an anisotropic and piezoelectric bimaterial full plane. By virtue of the equivalent body force and the line-source bimaterial Green functions, we first express the induced elastic and piezoelectric fields in terms of the boundary integral on the surface of the inclusion. The boundary integral is then carried out exactly in terms of simple and elementary functions by assuming that the boundary of the inclusion is made of piecewise straight-line segments. Since the solution is in an exact closed form, the induced elastic and piezoelectric fields due to multiple polygonal inclusions, in particular, due to the QWR array, can be simply superposed together. Benchmark numerical examples are also presented for the induced elastic and piezoelectric fields within a square inclusion due to a uniform hydrostatic eigenstrain, with the bimaterials being made of quartz and ceramic. Finally, we remark

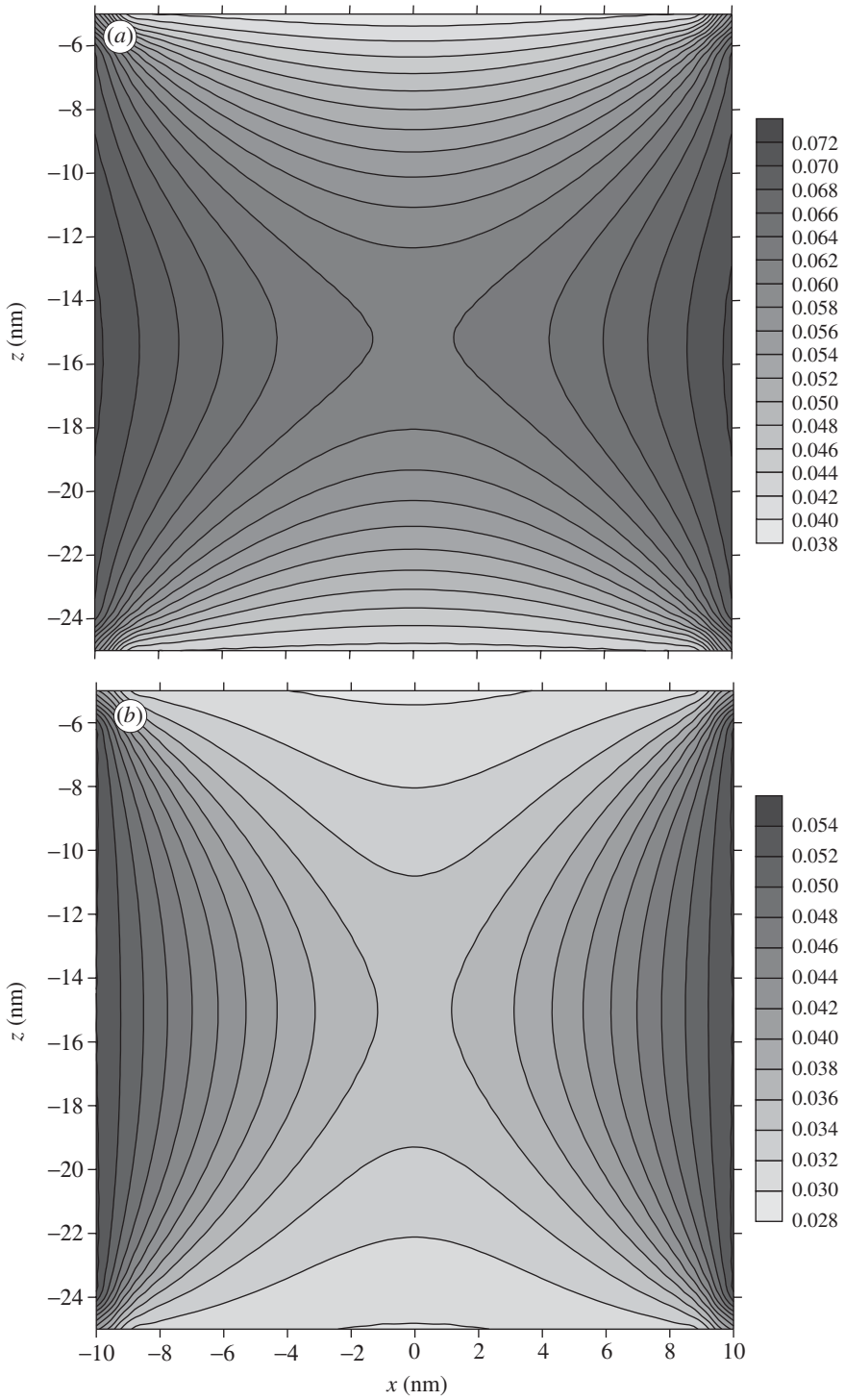

Figure 2. Contours of strain component γ_{xx} within the 20 nm × 20 nm square QWR in material 2 of (*a*) the quartz/ceramic bimaterials and (*b*) the ceramic/quartz bimaterials.

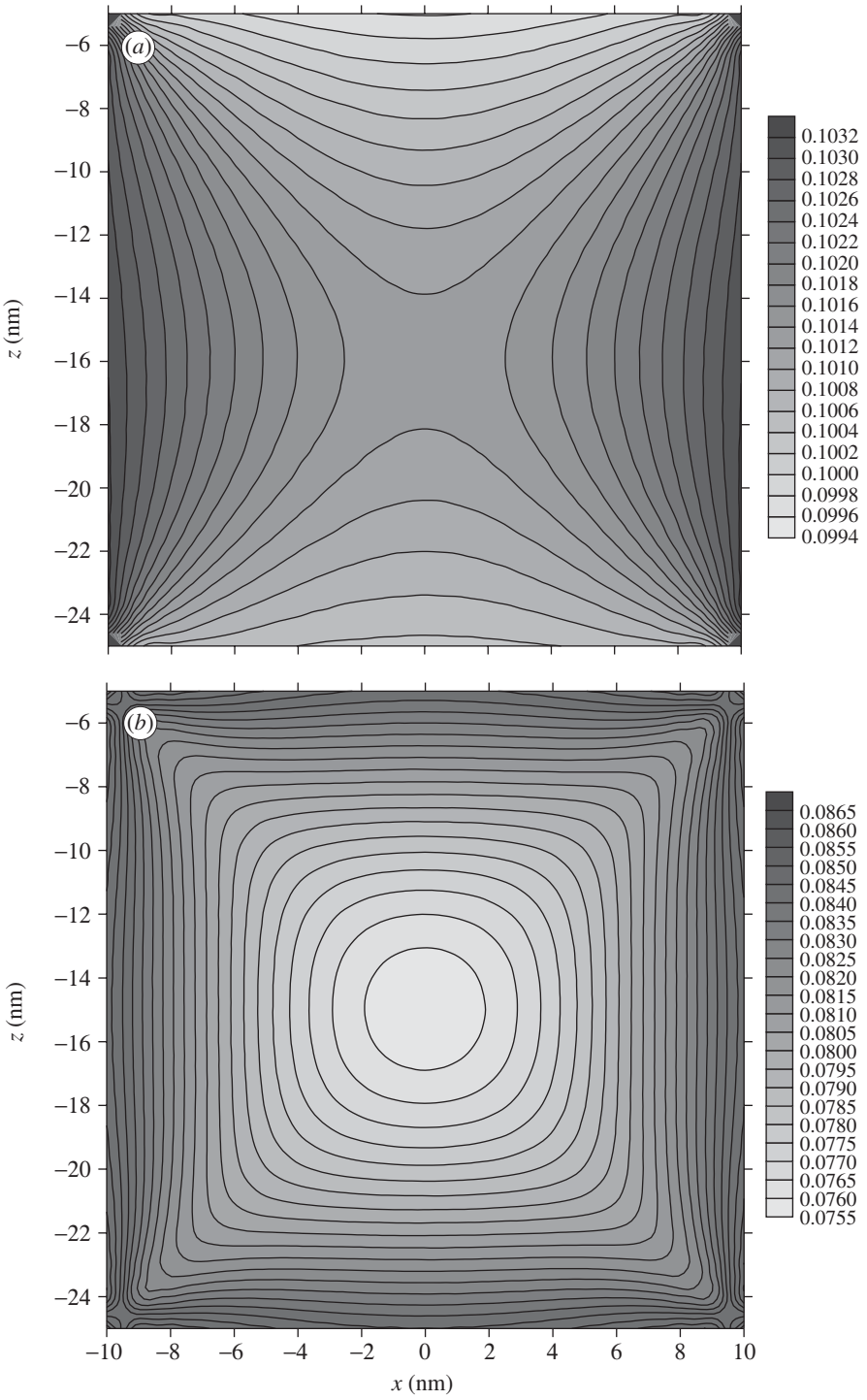

Figure 3. Contours of hydrostatic strain $\gamma_{xx} + \gamma_{zz}$ within the 20 nm × 20 nm square QWR in material 2 of (*a*) the quartz/ceramic bimaterials and (*b*) the ceramic/quartz bimaterials.

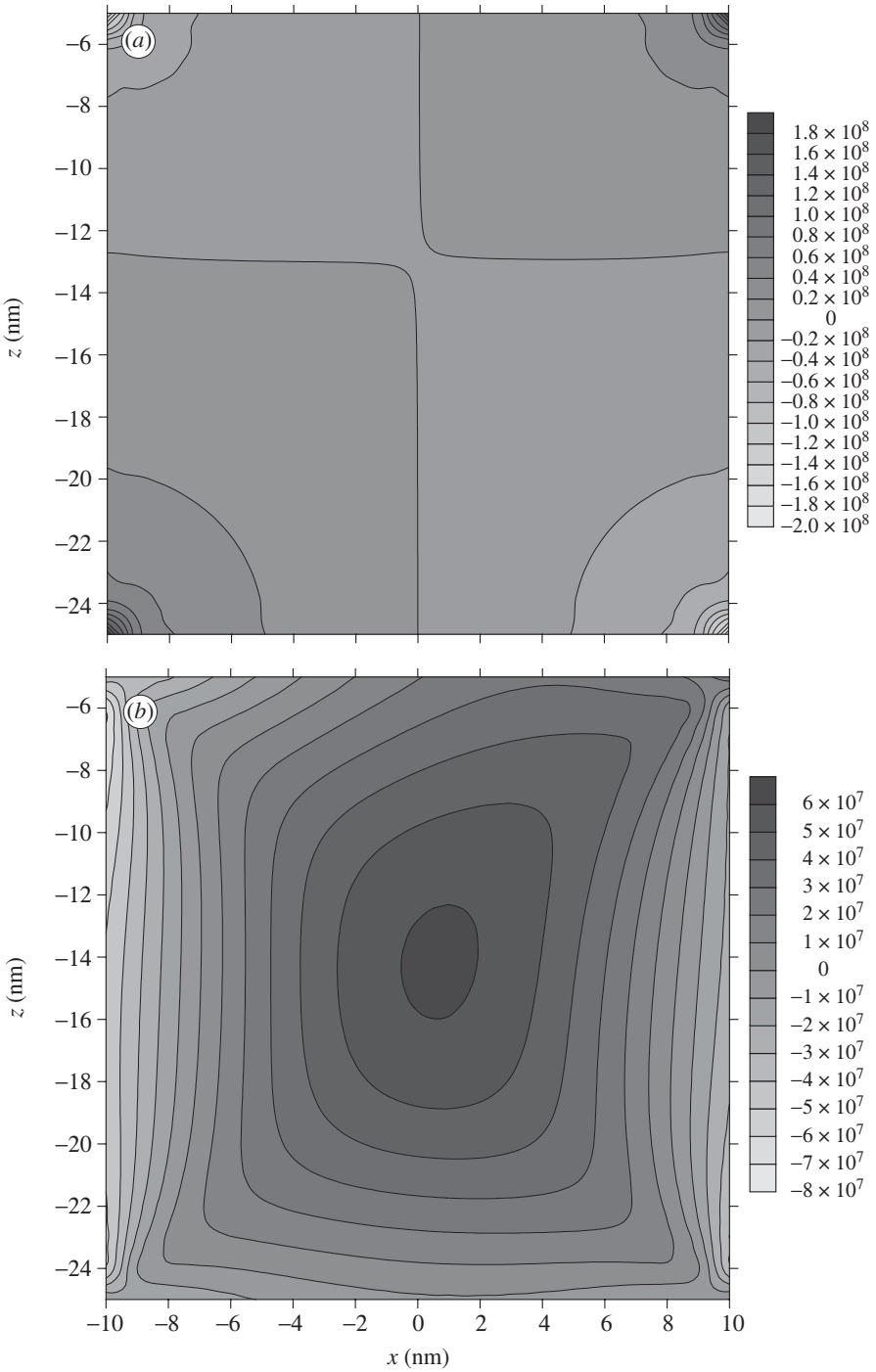

Figure 4. Contours of electric component E_x (V m^{-1}) within the 20 nm × 20 nm square QWR in material 2 of (a) the quartz/ceramic bimaterials and (b) the ceramic/quartz bimaterials.

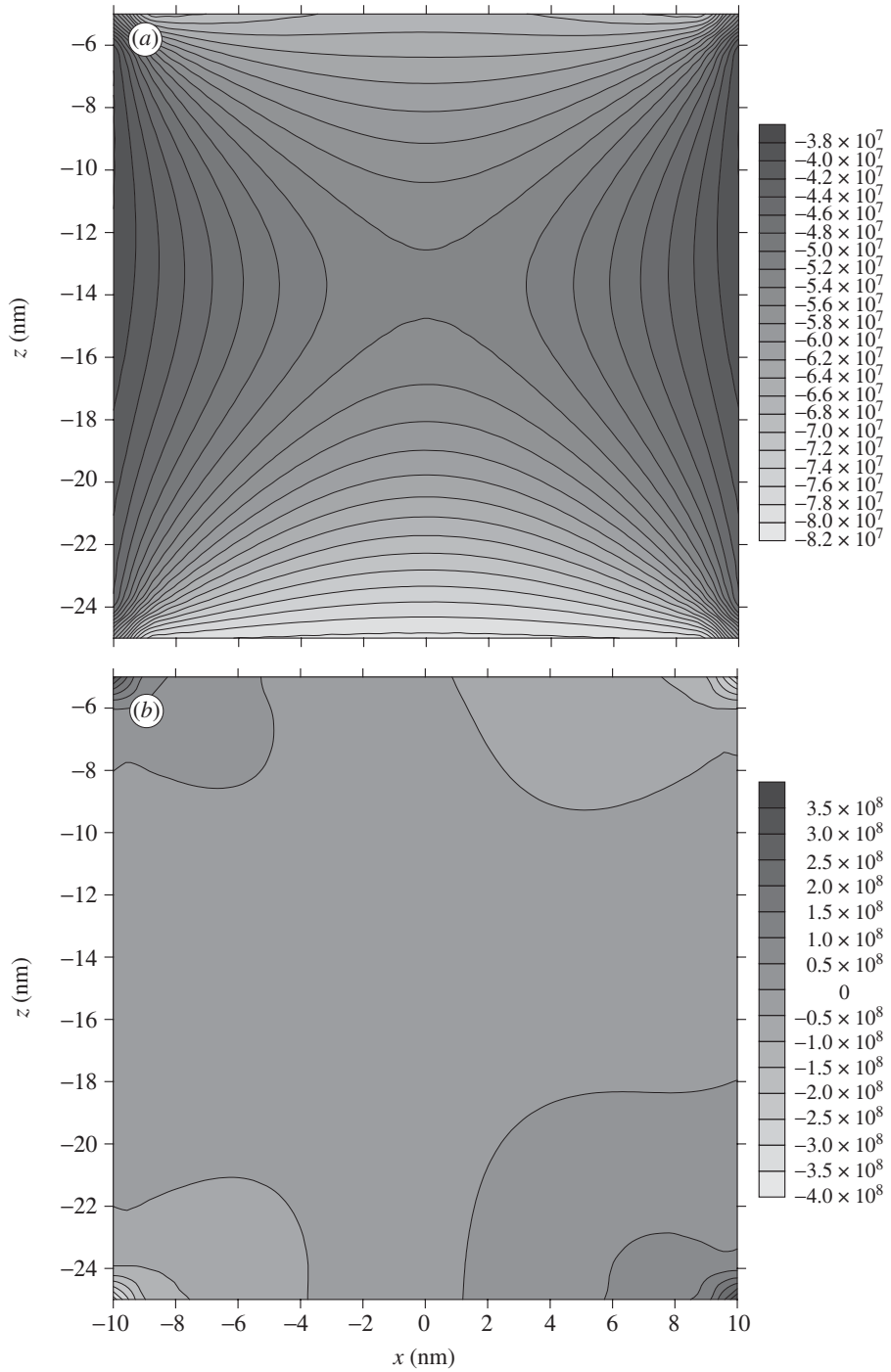

Figure 5. Contours of electric component E_z (V m^{-1}) within the 20 nm × 20 nm square QWR in material 2 of (*a*) the quartz/ceramic bimaterials and (*b*) the ceramic/quartz bimaterials.

that the present exact closed-form solution includes the solution to the corresponding anisotropic elastic bimaterials as its special case and, furthermore, contains a total of six different interface models which may be useful in the piezoelectric bimaterial analysis and design.

The author thanks both reviewers for their constructive comments, and the University of Akron for partial support under Grant no. 2-07522.

Appendix A. Five imperfect interface models and the corresponding modified matrices

Besides the perfect-bond interface model, the solution developed in the main text also applies to the following five imperfect interface models. What one needs to do is to replace some of the matrices with the modified ones. We now discuss these models one by one.

(*a*) *Model 2*

The mechanical displacement and traction vectors are continuous across the interface, and the electrical potential is zero along the interface, i.e.

$$\left.\begin{aligned} u_j^{(1)}|_{z=0^+} = u_j^{(2)}|_{z=0^-}, \qquad t_j^{(1)}|_{z=0^+} = t_j^{(2)}|_{z=0^-}, \quad j=1,2,3, \\ u_4^{(1)}|_{z=0^+} = u_4^{(2)}|_{z=0^-} = 0. \end{aligned}\right\} \tag{A 1}$$

We see that this interface is electrically closed (Alshits *et al*. 1994) or it is an electrical wall (see Papas 1988; Volakis *et al*. 1998). For this model, the modified matrices $\hat{\boldsymbol{A}}^{(\alpha)}$ and $\hat{\boldsymbol{B}}^{(\alpha)}$ in Appendix B are given as

$$\left.\begin{aligned} \hat{\boldsymbol{A}}^{(\alpha)} = \boldsymbol{A}^{(\alpha)}, \quad \alpha = 1,2, \\ \hat{\boldsymbol{B}}^{(1)} = \begin{pmatrix} B_{11}^{(1)} & B_{12}^{(1)} & B_{13}^{(1)} & B_{14}^{(1)} \\ B_{21}^{(1)} & B_{22}^{(1)} & B_{23}^{(1)} & B_{24}^{(1)} \\ B_{31}^{(1)} & B_{32}^{(1)} & B_{33}^{(1)} & B_{34}^{(1)} \\ A_{41}^{(1)} & A_{42}^{(1)} & A_{43}^{(1)} & A_{44}^{(1)} \end{pmatrix}, \\ \hat{\boldsymbol{B}}^{(2)} = \begin{pmatrix} B_{11}^{(2)} & B_{12}^{(2)} & B_{13}^{(2)} & B_{14}^{(2)} \\ B_{21}^{(2)} & B_{22}^{(2)} & B_{23}^{(2)} & B_{24}^{(2)} \\ B_{31}^{(2)} & B_{32}^{(2)} & B_{33}^{(2)} & B_{34}^{(2)} \\ -A_{41}^{(2)} & -A_{42}^{(2)} & -A_{43}^{(2)} & -A_{44}^{(2)} \end{pmatrix}. \end{aligned}\right\} \tag{A 2}$$

(*b*) *Model 3*

The mechanical displacement and traction vectors are continuous across the interface, and the normal electrical displacement is zero along the interface, i.e.

$$\left.\begin{aligned} u_j^{(1)}|_{z=0^+} = u_j^{(2)}|_{z=0^-}, \qquad t_j^{(1)}|_{z=0^+} = t_j^{(2)}|_{z=0^-}, \quad j=1,2,3, \\ t_4^{(1)}|_{z=0^+} = t_4^{(2)}|_{z=0^-} = 0. \end{aligned}\right\} \tag{A 3}$$

This interface is electrically open (Alshits *et al*. 1994) or it is a magnetic wall (see Papas 1988; Volakis *et al*. 1998). The modified matrices $\hat{\boldsymbol{A}}^{(\alpha)}$ and $\hat{\boldsymbol{B}}^{(\alpha)}$ are given as

$$\left.\begin{aligned}\hat{\boldsymbol{A}}^{(1)} &= \begin{pmatrix} A_{11}^{(1)} & A_{12}^{(1)} & A_{13}^{(1)} & A_{14}^{(1)} \\ A_{21}^{(1)} & A_{22}^{(1)} & A_{23}^{(1)} & A_{24}^{(1)} \\ A_{31}^{(1)} & A_{32}^{(1)} & A_{33}^{(1)} & A_{34}^{(1)} \\ B_{41}^{(1)} & B_{42}^{(1)} & B_{43}^{(1)} & B_{44}^{(1)} \end{pmatrix}, \\ \hat{\boldsymbol{A}}^{(2)} &= \begin{pmatrix} A_{11}^{(2)} & A_{12}^{(2)} & A_{13}^{(2)} & A_{14}^{(2)} \\ A_{21}^{(2)} & A_{22}^{(2)} & A_{23}^{(2)} & A_{24}^{(2)} \\ A_{31}^{(2)} & A_{32}^{(2)} & A_{33}^{(2)} & A_{34}^{(2)} \\ -B_{41}^{(2)} & -B_{42}^{(2)} & -B_{43}^{(2)} & -B_{44}^{(2)} \end{pmatrix}, \\ \hat{\boldsymbol{B}}^{(\alpha)} &= \boldsymbol{B}^{(\alpha)}, \quad \alpha = 1, 2. \end{aligned}\right\} \tag{A 4}$$

In these two models, as well as the perfect-bond interface model discussed in the main text, the mechanical displacement and traction vectors are assumed to be continuous across the interface, corresponding to the purely elastic bimaterials with perfect-bond interface condition. In the following three models, the mechanical perfect-bond condition is replaced by the mechanical smooth-bond or slippery condition.

(*c*) *Model 4*

Across the interface, the mechanical displacement and traction vectors are in smooth contact, and the electrical potential and normal electrical displacement component are continuous:

$$\left.\begin{aligned} u_m^{(1)}|_{z=0^+} = u_m^{(2)}|_{z=0^-}, \qquad t_m^{(1)}|_{z=0^+} = t_m^{(2)}|_{z=0^-}, \quad m = 3, 4, \\ t_\alpha^{(1)}|_{z=0^+} = t_\alpha^{(2)}|_{z=0^-} = 0, \quad \alpha = 1, 2. \end{aligned}\right\} \tag{A 5}$$

The modified matrices $\hat{\boldsymbol{A}}^{(\alpha)}$ and $\hat{\boldsymbol{B}}^{(\alpha)}$ are given as

$$\left.\begin{aligned}\hat{\boldsymbol{A}}^{(1)} &= \begin{pmatrix} B_{11}^{(1)} & B_{12}^{(1)} & B_{13}^{(1)} & B_{14}^{(1)} \\ B_{21}^{(1)} & B_{22}^{(1)} & B_{23}^{(1)} & B_{24}^{(1)} \\ A_{31}^{(1)} & A_{32}^{(1)} & A_{33}^{(1)} & A_{34}^{(1)} \\ A_{41}^{(1)} & A_{42}^{(1)} & A_{43}^{(1)} & A_{44}^{(1)} \end{pmatrix}, \\ \hat{\boldsymbol{A}}^{(2)} &= \begin{pmatrix} -B_{11}^{(2)} & -B_{12}^{(2)} & -B_{13}^{(2)} & -B_{14}^{(2)} \\ -B_{21}^{(2)} & -B_{22}^{(2)} & -B_{23}^{(2)} & -B_{24}^{(2)} \\ A_{31}^{(2)} & A_{32}^{(2)} & A_{33}^{(2)} & A_{34}^{(2)} \\ A_{41}^{(2)} & A_{42}^{(2)} & A_{43}^{(2)} & A_{44}^{(2)} \end{pmatrix}, \\ \hat{\boldsymbol{B}}^{(\alpha)} &= \boldsymbol{B}^{(\alpha)}, \quad \alpha = 1, 2. \end{aligned}\right\} \tag{A 6}$$

(*d*) *Model 5*

Across the interface the mechanical displacement and traction vectors are in smooth contact, and along the interface the electrical potential is zero:

$$\left.\begin{gathered} u_3^{(1)}|_{z=0^+} = u_3^{(2)}|_{z=0^-}, \qquad t_3^{(1)}|_{z=0^+} = t_3^{(2)}|_{z=0^-}, \\ t_\alpha^{(1)}|_{z=0^+} = t_\alpha^{(2)}|_{z=0^-} = 0, \quad \alpha = 1,2, \\ u_4^{(1)}|_{z=0^+} = u_4^{(2)}|_{z=0^-} = 0. \end{gathered}\right\} \tag{A 7}$$

The modified matrices $\hat{\boldsymbol{A}}^{(\alpha)}$ and $\hat{\boldsymbol{B}}^{(\alpha)}$ are given as

$$\left.\begin{aligned} \hat{\boldsymbol{A}}^{(1)} &= \begin{pmatrix} B_{11}^{(1)} & B_{12}^{(1)} & B_{13}^{(1)} & B_{14}^{(1)} \\ B_{21}^{(1)} & B_{22}^{(1)} & B_{23}^{(1)} & B_{24}^{(1)} \\ A_{31}^{(1)} & A_{32}^{(1)} & A_{33}^{(1)} & A_{34}^{(1)} \\ A_{41}^{(1)} & A_{42}^{(1)} & A_{43}^{(1)} & A_{44}^{(1)} \end{pmatrix}, \\ \hat{\boldsymbol{A}}^{(2)} &= \begin{pmatrix} -B_{11}^{(2)} & -B_{12}^{(2)} & -B_{13}^{(2)} & -B_{14}^{(2)} \\ -B_{21}^{(2)} & -B_{22}^{(2)} & -B_{23}^{(2)} & -B_{24}^{(2)} \\ A_{31}^{(2)} & A_{32}^{(2)} & A_{33}^{(2)} & A_{34}^{(2)} \\ -A_{41}^{(2)} & -A_{42}^{(2)} & -A_{43}^{(2)} & -A_{44}^{(2)} \end{pmatrix}, \\ \hat{\boldsymbol{B}}^{(1)} &= \begin{pmatrix} B_{11}^{(1)} & B_{12}^{(1)} & B_{13}^{(1)} & B_{14}^{(1)} \\ B_{21}^{(1)} & B_{22}^{(1)} & B_{23}^{(1)} & B_{24}^{(1)} \\ B_{31}^{(1)} & B_{32}^{(1)} & B_{33}^{(1)} & B_{34}^{(1)} \\ A_{41}^{(1)} & A_{42}^{(1)} & A_{43}^{(1)} & A_{44}^{(1)} \end{pmatrix}, \\ \hat{\boldsymbol{B}}^{(2)} &= \begin{pmatrix} B_{11}^{(2)} & B_{12}^{(2)} & B_{13}^{(2)} & B_{14}^{(2)} \\ B_{21}^{(2)} & B_{22}^{(2)} & B_{23}^{(2)} & B_{24}^{(2)} \\ B_{31}^{(2)} & B_{32}^{(2)} & B_{33}^{(2)} & B_{34}^{(2)} \\ A_{41}^{(2)} & A_{42}^{(2)} & A_{43}^{(2)} & A_{44}^{(2)} \end{pmatrix}. \end{aligned}\right\} \tag{A 8}$$

(*e*) *Model 6*

Across the interface the mechanical displacement and traction vectors are in smooth contact, and along the interface the normal electrical displacement component is zero:

$$\left.\begin{gathered} u_3^{(1)}|_{z=0^+} = u_3^{(2)}|_{z=0^-}, \qquad t_3^{(1)}|_{z=0^+} = t_3^{(2)}|_{z=0^-}, \\ t_\alpha^{(1)}|_{z=0^+} = t_\alpha^{(2)}|_{z=0^-} = 0, \quad \alpha = 1,2, \\ t_4^{(1)}|_{z=0^+} = t_4^{(2)}|_{z=0^-} = 0. \end{gathered}\right\} \tag{A 9}$$

The modified matrices $\hat{\boldsymbol{A}}^{(\alpha)}$ and $\hat{\boldsymbol{B}}^{(\alpha)}$ are given as

$$\left.\begin{aligned}\hat{\boldsymbol{A}}^{(1)} &= \begin{pmatrix} B_{11}^{(1)} & B_{12}^{(1)} & B_{13}^{(1)} & B_{14}^{(1)} \\ B_{21}^{(1)} & B_{22}^{(1)} & B_{23}^{(1)} & B_{24}^{(1)} \\ A_{31}^{(1)} & A_{32}^{(1)} & A_{33}^{(1)} & A_{34}^{(1)} \\ B_{41}^{(1)} & B_{42}^{(1)} & B_{43}^{(1)} & B_{44}^{(1)} \end{pmatrix}, \\ \hat{\boldsymbol{A}}^{(2)} &= \begin{pmatrix} -B_{11}^{(2)} & -B_{12}^{(2)} & -B_{13}^{(2)} & -B_{14}^{(2)} \\ -B_{21}^{(2)} & -B_{22}^{(2)} & -B_{23}^{(2)} & -B_{24}^{(2)} \\ A_{31}^{(2)} & A_{32}^{(2)} & A_{33}^{(2)} & A_{34}^{(2)} \\ -B_{41}^{(2)} & -B_{42}^{(2)} & -B_{43}^{(2)} & -B_{44}^{(2)} \end{pmatrix}, \\ \hat{\boldsymbol{B}}^{(\alpha)} &= \boldsymbol{B}^{(\alpha)}, \quad \alpha = 1, 2. \end{aligned}\right\} \tag{A 10}$$

Appendix B. 2D piezoelectric bimaterial Green functions due to line force and dislocation

We consider an anisotropic and piezoelectric bimaterial full-space made of two half-spaces with an interface at $z = 0$. Let us assume that materials 1 and 2 occupy the upper ($z > 0$) and lower ($z < 0$) half-spaces, respectively. Here, however, it is required that the deformation is independent of the y-coordinate (i.e. the generalized plane-strain deformation in the (x, z)-plane). We further let an extended line force $\boldsymbol{f} = (f_1, f_2, f_3, -q)^t$ and an extended line dislocation (i.e. a Burgers vector) $\boldsymbol{b} = (\Delta u_1, \Delta u_2, \Delta u_3, \Delta\phi)^t$ be applied at $(x, z) = (X, Z)$ in material 1 or 2.

Similar to the purely elastic bimaterial case (Ting 1996), it can be shown that the analytical bimaterial Green functions (i.e. the extended displacements and stress functions) can be derived using the Stroh formalism.

For the source point in material 1 ($Z > 0$), we have

$$\left.\begin{aligned}\boldsymbol{u}^{(1)} &= \frac{1}{\pi}\,\mathrm{Im}\{\boldsymbol{A}^{(1)}\langle\ln(z_*^{(1)} - s_*^{(1)})\rangle\boldsymbol{q}^{\infty,1}\} + \frac{1}{\pi}\,\mathrm{Im}\sum_{J=1}^{4}\{\boldsymbol{A}^{(1)}\langle\ln(z_*^{(1)} - \bar{s}_J^{(1)})\rangle\boldsymbol{q}_J^{(1)}\}, \\ \boldsymbol{\psi}^{(1)} &= \frac{1}{\pi}\,\mathrm{Im}\{\boldsymbol{B}^{(1)}\langle\ln(z_*^{(1)} - s_*^{(1)})\rangle\boldsymbol{q}^{\infty,1}\} + \frac{1}{\pi}\,\mathrm{Im}\sum_{J=1}^{4}\{\boldsymbol{B}^{(1)}\langle\ln(z_*^{(1)} - \bar{s}_J^{(1)})\rangle\boldsymbol{q}_J^{(1)}\},\end{aligned}\right\} \tag{B 1}$$

for field point in material 1 ($z > 0$), and

$$\left.\begin{aligned}\boldsymbol{u}^{(2)} &= \frac{1}{\pi}\,\mathrm{Im}\sum_{J=1}^{4}\{\boldsymbol{A}^{(2)}\langle\ln(z_*^{(2)} - s_J^{(1)})\rangle\boldsymbol{q}_J^{(2)}\}, \\ \boldsymbol{\psi}^{(2)} &= \frac{1}{\pi}\,\mathrm{Im}\sum_{J=1}^{4}\{\boldsymbol{B}^{(2)}\langle\ln(z_*^{(2)} - s_J^{(1)})\rangle\boldsymbol{q}_J^{(2)}\},\end{aligned}\right\} \tag{B 2}$$

for field point in material 2 ($z < 0$).

In equations (B 1) and (B 2), $\boldsymbol{\psi}$ is the extended stress function vector related to the elastic stresses and electrical displacements by

$$\sigma_{1J} = -\psi_{J,3}; \qquad \sigma_{3J} = \psi_{J,1}. \tag{B 3}$$

Also in equations (B 1) and (B 2), 'Im' stands for the imaginary part, and the superscripts '(1)' and '(2)' denote, as in the text, the quantities associated with the material domains 1 and 2, respectively; $p_J^{(\alpha)}$, $\boldsymbol{A}^{(\alpha)}$, and $\boldsymbol{B}^{(\alpha)}$ are the Stroh eigenvalues and matrices. They are solutions of the eigenequation discussed in Appendix A of Pan (2004). Finally, in equations (B 1) and (B 2),

$$\left.\begin{aligned}
&\langle \ln(z_*^{(1)} - s_*^{(1)})\rangle \\
&\quad = \operatorname{diag}[\ln(z_1^{(1)} - s_1^{(1)}), \ln(z_2^{(1)} - s_2^{(1)}), \ln(z_3^{(1)} - s_3^{(1)}), \ln(z_4^{(1)} - s_4^{(1)})], \\
&\langle \ln(z_*^{(\alpha)} - \bar{s}_J^{(1)})\rangle \\
&\quad = \operatorname{diag}[\ln(z_1^{(\alpha)} - \bar{s}_J^{(1)}), \ln(z_2^{(\alpha)} - \bar{s}_J^{(1)}), \ln(z_3^{(\alpha)} - \bar{s}_J^{(1)}), \ln(z_4^{(\alpha)} - \bar{s}_J^{(1)})] \\
&\qquad\qquad\qquad\qquad\qquad\qquad\qquad\qquad\qquad\qquad (\alpha = 1, 2),
\end{aligned}\right\} \tag{B 4}$$

with the complex variable $z_J^{(\alpha)}$and $s_J^{(\alpha)}$ being defined by

$$z_J^{(\alpha)} = x + p_J^{(\alpha)} z, \tag{B 5}$$

$$s_J^{(\alpha)} = X + p_J^{(\alpha)} Z. \tag{B 6}$$

Note that the first term in equation (B 1) corresponds to the full-plane Green functions (with material properties of material 1) with

$$\boldsymbol{q}^{\infty,1} = (\boldsymbol{A}^{(1)})^{\mathrm{T}} \boldsymbol{f} + (\boldsymbol{B}^{(1)})^{\mathrm{T}} \boldsymbol{b}. \tag{B 7}$$

The second term in equation (B 1) and the solution in material 2 (B 2) are the complementary parts of the solution with the complex constant vectors $\boldsymbol{q}_J^{(\alpha)}$ ($\alpha = 1, 2$, $J = 1, 2, 3, 4$) to be determined.

For a perfect-bond interface at $z = 0$, it can be shown that the constant vectors $\boldsymbol{q}_J^{(\alpha)}$ satisfy the conditions ($J = 1, 2, 3, 4$)

$$\left.\begin{aligned}
\boldsymbol{A}^{(1)} \boldsymbol{q}_J^{(1)} + \bar{\boldsymbol{A}}^{(2)} \bar{\boldsymbol{q}}_J^{(2)} &= \bar{\boldsymbol{A}}^{(1)} \boldsymbol{I}_J \bar{\boldsymbol{q}}^{\infty,1}, \\
\boldsymbol{B}^{(1)} \boldsymbol{q}_J^{(1)} + \bar{\boldsymbol{B}}^{(2)} \bar{\boldsymbol{q}}_J^{(2)} &= \bar{\boldsymbol{B}}^{(1)} \boldsymbol{I}_J \bar{\boldsymbol{q}}^{\infty,1},
\end{aligned}\right\} \tag{B 8}$$

with

$$\left.\begin{aligned}
\boldsymbol{I}_1 &= \operatorname{diag}[1, 0, 0, 0], & \boldsymbol{I}_2 &= \operatorname{diag}[0, 1, 0, 0], \\
\boldsymbol{I}_3 &= \operatorname{diag}[0, 0, 1, 0], & \boldsymbol{I}_4 &= \operatorname{diag}[0, 0, 0, 1].
\end{aligned}\right\} \tag{B 9}$$

The solutions of the vectors are readily found to be

$$\left.\begin{aligned}
\boldsymbol{q}_J^{(1)} &= (\boldsymbol{A}^{(1)})^{-1} (\boldsymbol{M}^{(1)} + \bar{\boldsymbol{M}}^{(2)})^{-1} (\bar{\boldsymbol{M}}^{(2)} - \bar{\boldsymbol{M}}^{(1)}) \bar{\boldsymbol{A}}^{(1)} \boldsymbol{I}_J \bar{\boldsymbol{q}}^{\infty,1}, \\
\boldsymbol{q}_J^{(2)} &= (\boldsymbol{A}^{(2)})^{-1} (\bar{\boldsymbol{M}}^{(1)} + \boldsymbol{M}^{(2)})^{-1} (\boldsymbol{M}^{(1)} + \bar{\boldsymbol{M}}^{(1)}) \boldsymbol{A}^{(1)} \boldsymbol{I}_J \boldsymbol{q}^{\infty,1},
\end{aligned}\right\} \tag{B 10}$$

where $\boldsymbol{M}^{(\alpha)}$ are the impedance tensors, defined as

$$\boldsymbol{M}^{(\alpha)} = -\mathrm{i} \boldsymbol{B}^{(\alpha)} (\boldsymbol{A}^{(\alpha)})^{-1}, \quad \alpha = 1, 2. \tag{B 11}$$

The complex constants involved in the bimaterial Green solutions (B 1) and (B 2) for the five interface models discussed in Appendix A can also be determined by following the same procedure. As in equation (B 10), the solutions can be written as

$$\left.\begin{aligned} \boldsymbol{q}_J^{(1)} &= (\hat{\boldsymbol{A}}^{(1)})^{-1}(\hat{\boldsymbol{M}}^{(1)} + \bar{\hat{\boldsymbol{M}}}^{(2)})^{-1}(\bar{\hat{\boldsymbol{M}}}^{(2)} - \bar{\hat{\boldsymbol{M}}}^{(1)}\bar{\hat{\boldsymbol{A}}}^{(1)}\boldsymbol{I}_J\bar{\boldsymbol{q}}^{\infty,1} \\ &\equiv \boldsymbol{K}^{11}\boldsymbol{I}_J\bar{\boldsymbol{q}}^{\infty,1}, \\ \boldsymbol{q}_J^{(2)} &= (\hat{\boldsymbol{A}}^{(2)})^{-1}(\bar{\hat{\boldsymbol{M}}}^{(1)} + \hat{\boldsymbol{M}}^{(2)})^{-1}(\hat{\boldsymbol{M}}^{(1)} + \bar{\hat{\boldsymbol{M}}}^{(1)})\hat{\boldsymbol{A}}^{(1)}\boldsymbol{I}_J q^{\infty,1} \\ &\equiv \boldsymbol{K}^{12}\boldsymbol{I}_J\boldsymbol{q}^{\infty,1}, \end{aligned}\right\} \tag{B 12}$$

where $\hat{\boldsymbol{M}}^{(\alpha)}$ $(\alpha = 1, 2)$ are the modified impedance tensors defined as

$$\hat{\boldsymbol{M}}^{(\alpha)} = -\mathrm{i}\hat{\boldsymbol{B}}^{(\alpha)}(\hat{\boldsymbol{A}}^{(\alpha)})^{-1}, \quad \alpha = 1, 2, \tag{B 13}$$

and the modified matrices $\hat{\boldsymbol{A}}^{(\alpha)}$ and $\hat{\boldsymbol{B}}^{(\alpha)}$ $(\alpha = 1, 2)$ are given in Appendix A for the five imperfect interface models. Equation (B 12) is for the five imperfect interface models as well as for the perfect-bond interface model 1. For the perfect-bond interface case, we simply have

$$\hat{\boldsymbol{A}}^{(\alpha)} = \boldsymbol{A}^{(\alpha)}, \qquad \hat{\boldsymbol{B}}^{(\alpha)} = \boldsymbol{B}^{(\alpha)}, \quad \alpha = 1, 2. \tag{B 14}$$

Taking only the line-force contribution in (B 7) and writing the Green function solution in terms of the 4×4 matrix, we found

$$\left.\begin{aligned} Q_{RN}^{11,v} &= K_{RP}^{11}(\boldsymbol{I}_v)_P\bar{A}_{NP}^{(1)}, \\ Q_{RN}^{12,v} &= K_{RP}^{12}(\boldsymbol{I}_v)_P A_{NP}^{(1)}. \end{aligned}\right\} \tag{B 15}$$

Similarly, for the source point in material 2 $(Z < 0)$, we have

$$\left.\begin{aligned} \boldsymbol{u}^{(1)} &= \frac{1}{\pi}\,\mathrm{Im}\sum_{J=1}^{4}\{\boldsymbol{A}^{(1)}\langle\ln(z_*^{(1)} - s_J^{(2)})\rangle\boldsymbol{q}_J^{(1)}\}, \\ \boldsymbol{\psi}^{(1)} &= \frac{1}{\pi}\,\mathrm{Im}\sum_{J=1}^{4}\{\boldsymbol{B}^{(1)}\langle\ln(z_*^{(1)} - s_J^{(2)})\rangle\boldsymbol{q}_J^{(1)}\}, \end{aligned}\right\} \tag{B 16}$$

for the field point in material 1 $(z > 0)$, and

$$\left.\begin{aligned} \boldsymbol{u}^{(2)} &= \frac{1}{\pi}\,\mathrm{Im}\{\boldsymbol{A}^{(2)}\langle\ln(z_*^{(2)} - s_*^{(2)})\rangle\boldsymbol{q}^{\infty,2}\} + \frac{1}{\pi}\,\mathrm{Im}\sum_{J=1}^{4}\{\boldsymbol{A}^{(2)}\langle\ln(z_*^{(2)} - \bar{s}_J^{(2)})\rangle\boldsymbol{q}_J^{(2)}\}, \\ \boldsymbol{\psi}^{(2)} &= \frac{1}{\pi}\,\mathrm{Im}\{\boldsymbol{B}^{(2)}\langle\ln(z_*^{(2)} - s_*^{(2)})\rangle\boldsymbol{q}^{\infty,2}\} + \frac{1}{\pi}\,\mathrm{Im}\sum_{J=1}^{4}\{\boldsymbol{B}^{(2)}\langle\ln(z_*^{(2)} - \bar{s}_J^{(2)})\rangle\boldsymbol{q}_J^{(2)}\}, \end{aligned}\right\} \tag{B 17}$$

for field point in $z < 0$ (material 2).

Note again that the first term in equation (B 17) corresponds to the full-plane Green functions (with material properties of material 2) with

$$\boldsymbol{q}^{\infty,2} = (\boldsymbol{A}^{(2)})^{\mathrm{T}}\boldsymbol{f} + (\boldsymbol{B}^{(2)})^{\mathrm{T}}b. \tag{B 18}$$

For the six interface models, we found that

$$\left.\begin{aligned} \boldsymbol{q}_J^{(1)} &= (\hat{\boldsymbol{A}}^{(1)})^{-1}(\bar{\hat{\boldsymbol{M}}}^{(2)} + \hat{\boldsymbol{M}}^{(1)})^{-1}(\hat{\boldsymbol{M}}^{(2)} + \bar{\hat{\boldsymbol{M}}}^{(2)})\hat{\boldsymbol{A}}^{(2)}\boldsymbol{I}_J\boldsymbol{q}^{\infty,2} \\ &\equiv \boldsymbol{K}^{21}\boldsymbol{I}_J\boldsymbol{q}^{\infty,2}, \\ \boldsymbol{q}_J^{(2)} &= (\hat{\boldsymbol{A}}^{(2)})^{-1}(\hat{\boldsymbol{M}}^{(2)} + \bar{\hat{\boldsymbol{M}}}^{(1)})^{-1}(\bar{\hat{\boldsymbol{M}}}^{(1)} - \bar{\hat{\boldsymbol{M}}}^{(2)})\bar{\hat{\boldsymbol{A}}}^{(2)}\boldsymbol{I}_J\bar{\boldsymbol{q}}^{\infty,2} \\ &\equiv \boldsymbol{K}^{22}\boldsymbol{I}_J\bar{\boldsymbol{q}}^{\infty,2}, \end{aligned}\right\} \tag{B 19}$$

$$\left.\begin{aligned} Q_{RN}^{21,v} &= K_{RP}^{21}(\boldsymbol{I}_v)_P A_{NP}^{(2)}, \\ Q_{RN}^{22,v} &= K_{RP}^{22}(\boldsymbol{I}_v)_P \bar{A}_{NP}^{(2)}. \end{aligned}\right\} \tag{B 20}$$

Appendix C. Some analytical integrals

For the $h_R^{(\alpha)}$ defined in (4.5) in the text, we write $z_R^{(\alpha)}$ in terms of the parameter t in (4.3) and find that

$$h_R^{(\alpha)}(X,Z) = \int_0^1 \ln\{[(x_2-x_1) + p_R^{(\alpha)}(z_2-z_1)]t + [(x_1 + p_R^{(\alpha)}z_1) - s_R^{(\alpha)}]\}\,\mathrm{d}t. \tag{C 1}$$

Integration of this expression gives

$$h_R^{(\alpha)}(X,Z) = \frac{(x_1 + p_R^{(\alpha)}z_1) - s_R^{(\alpha)}}{(x_2-x_1) + p_R^{(\alpha)}(z_2-z_1)} \ln\left[\frac{x_2 + p_R^{(\alpha)}z_2 - s_R^{(\alpha)}}{x_1 + p_R^{(\alpha)}z_1 - s_R^{(\alpha)}}\right] + \ln[x_2 + p_R^{(\alpha)}z_2 - s_R^{(\alpha)}] - 1. \tag{C 2}$$

Similarly, integration of $g_{Rv}^{\alpha\beta}$ and $w_{Rv}^{(\alpha)}$ gives

$$\left.\begin{aligned} g_{Rv}^{\alpha\beta}(X,Z) &= \frac{(x_1 + p_R^{(\alpha)}z_1) - s_v^{(\beta)}}{(x_2-x_1) + p_R^{(\alpha)}(z_2-z_1)} \ln\left[\frac{x_2 + p_R^{(\alpha)}z_2 - s_v^{(\beta)}}{x_1 + p_R^{(\alpha)}z_1 - s_v^{(\beta)}}\right] + \ln[x_2 + p_R^{(\alpha)}z_2 - s_v^{(\beta)}] - 1, \\ w_{Rv}^{(\alpha)}(X,Z) &= \frac{(x_1 + p_R^{(\alpha)}z_1) - \bar{s}_v^{(\alpha)}}{(x_2-x_1) + p_R^{(\alpha)}(z_2-z_1)} \ln\left[\frac{x_2 + p_R^{(\alpha)}z_2 - \bar{s}_v^{(\alpha)}}{x_1 + p_R^{(\alpha)}z_1 - \bar{s}_v^{(\alpha)}}\right] + \ln[x_2 + p_R^{(\alpha)}z_2 - \bar{s}_v^{(\alpha)}] - 1. \end{aligned}\right\} \tag{C 3}$$

Taking the derivative of equations (C 2) and (C 3) with respect to the source coordinates X and Z (for subscripts '1' and '3', respectively), we find

$$h_{R,1}^{(\alpha)}(X,Z) = \frac{-1}{(x_2-x_1) + p_R^{(\alpha)}(z_2-z_1)} \ln\left[\frac{x_2 + p_R^{(\alpha)}z_2 - s_R^{(\alpha)}}{x_1 + p_R^{(\alpha)}z_1 - s_R^{(\alpha)}}\right], \tag{C 4}$$

$$h_{R,3}^{(\alpha)}(X,Z) = \frac{-p_R^{(\alpha)}}{(x_2-x_1) + p_R^{(\alpha)}(z_2-z_1)} \ln\left[\frac{x_2 + p_R^{(\alpha)}z_2 - s_R^{(\alpha)}}{x_1 + p_R^{(\alpha)}z_1 - s_R^{(\alpha)}}\right], \tag{C 5}$$

$$g^{\alpha\beta}_{Rv,1}(X,Z) = \frac{-1}{(x_2-x_1)+p_R^{(\alpha)}(z_2-z_1)} \ln\left[\frac{x_2+p_R^{(\alpha)}z_2-s_v^{(\beta)}}{x_1+p_R^{(\alpha)}z_1-s_v^{(\beta)}}\right], \tag{C 6}$$

$$g^{\alpha\beta}_{Rv,3}(X,Z) = \frac{-p_v^{(\beta)}}{(x_2-x_1)+p_R^{(\alpha)}(z_2-z_1)} \ln\left[\frac{x_2+p_R^{(\alpha)}z_2-s_v^{(\beta)}}{x_1+p_R^{(\alpha)}z_1-s_v^{(\beta)}}\right], \tag{C 7}$$

$$w^{(\alpha)}_{Rv,1}(X,Z) = \frac{-1}{(x_2-x_1)+p_R^{(\alpha)}(z_2-z_1)} \ln\left[\frac{x_2+p_R^{(\alpha)}z_2-\bar{s}_v^{(\alpha)}}{x_1+p_R^{(\alpha)}z_1-\bar{s}_v^{(\alpha)}}\right], \tag{C 8}$$

$$w^{(\alpha)}_{Rv,3}(X,Z) = \frac{-\bar{p}_v^{(\alpha)}}{(x_2-x_1)+p_R^{(\alpha)}(z_2-z_1)} \ln\left[\frac{x_2+p_R^{(\alpha)}z_2-\bar{s}_v^{(\alpha)}}{x_1+p_R^{(\alpha)}z_1-\bar{s}_v^{(\alpha)}}\right]. \tag{C 9}$$

References

Alshits, V. I., Barnett, D. M., Darinskii, A. N. & Lothe, J. 1994 On the existence problem for localized acoustic waves on the interface between two piezocrystals. *Wave Motion* **20**, 233–244.

Bacon, D. J., Barnett, D. M. & Scattergood, R. O. 1978 The anisotropic continuum theory of lattice defects. *Prog. Mater. Sci.* **23**, 51–262.

Barnett, D. M. & Lothe, J. 1975 Dislocations and line charges in anisotropic piezoelectric insulators. *Physica Status Solidi* B **67**, 105–111.

Bimberg, D., Grundmann, M. & Ledentsov, N. N. 1999 *Quantum dot heterostructures*. Wiley.

Buryachenko, V. A. 2001 Multiparticle effective field and related methods in micromechanics of composite materials. *Appl. Mech. Rev.* **54**, 1–47.

Davies, J. H. 1998*a* *The physics of low-dimensional semiconductors: an introduction*. Cambridge University Press.

Davies, J. H. 1998*b* Elastic and piezoelectric fields around a buried quantum dot: a simple picture. *J. Appl. Phys.* **84**, 1358–1365.

Davies, J. H. & Larkin, I. A. 1994 Theory of potential modulation in lateral surface superlattices. *Phys. Rev.* B **49**, 4800–4809.

Downes, J. R., Faux, D. A. & O'Reilly, E. P. 1995 Influence of strain relaxation on the electronic properties of buried quantum wells and wires. *Mater. Sci. Engng* B **35**, 357–363.

Dunn, M. L. & Taya, M. 1993 An analysis of piezoelectric composite materials containing ellipsoidal inhomogeneities. *Proc. R. Soc. Lond.* A **443**, 265–287.

Eshelby, J. D. 1957 The determination of the elastic field of an ellipsoidal inclusion, and related problems. *Proc. R. Soc. Lond.* A **241**, 376–396.

Eshelby, J. D. 1959 The elastic field outside an ellipsoidal inclusion. *Proc. R. Soc. Lond.* A **252**, 561–569.

Eshelby, J. D. 1961 Elastic inclusions and inhomogeneities. In *Progress in solid mechanics* (ed. I. N. Sneddon & R. Hill), vol. 2, pp. 89–140. Amsterdam: North-Holland.

Faux, D. A. & Pearson, G. S. 2000 Green's tensors for anisotropic elasticity: application to quantum dots. *Phys. Rev.* B **62**, R4798–R4801.

Faux, D. A., Downes, J. R. & O'Reilly, E. P. 1997 Analytic solutions for strain distribution in quantum-wire structures. *J. Appl. Phys.* **82**, 3754–3762.

Freund, L. B. & Johnson, H. T. 2001 Influence of strain on functional characteristics of nanoelectronic devices. *J. Mech. Phys. Solids* **49**, 1925–1935.

Glas, F. 2001 Elastic relaxation of truncated pyramidal quantum dots and quantum wires in a half-space: an analytical calculation. *J. Appl. Phys.* **90**, 3232–3241.

Glas, F. 2002 Analytical calculation of the strain field of single and periodic misfitting polygonal wires in a half-space. *Phil. Mag.* A **82**, 2591–2608.

Gosling, T. J. & Willis, J. R. 1995 Mechanical stability and electronic properties of buried strained quantum wire arrays. *J. Appl. Phys.* **77**, 5601–5610.

Jogai, B. 2001 Three-dimensional strain field calculations in multiple InN/AlN wurtzite quantum dots. *J. Appl. Phys.* **90**, 699–704.

Mura, T. 1987 *Micromechanics of defects in solids*, 2nd edn. Dordrecht: Kluwer.

Pan, E. 1999 A BEM analysis of fracture mechanics in 2D anisotropic piezoelectric solids. *Engng Analysis Bound. Elem.* **23**, 67–76.

Pan, E. 2002*a* Elastic and piezoelectric fields around a quantum dot: fully coupled or semi-coupled model. *J. Appl. Phys.* **91**, 3785–3796.

Pan, E. 2002*b* Elastic and piezoelectric fields in substrates GaAs (001) and GaAs (111) due to a buried quantum dot. *J. Appl. Phys.* **91**, 6379–6387.

Pan, E. 2002*c* Mindlin's problem for an anisotropic piezoelectric half space with general boundary conditions. *Proc. R. Soc. Lond.* A **458**, 181–208.

Pan, E. 2004 Eshelby problem of polygonal inclusions in anisotropic piezoelectric full- and half-planes. *J. Mech. Phys. Solids*. (In the press.)

Pan, E. & Yang, B. 2003 Elastic and piezoelectric fields in a substrate AlN due to a buried quantum dot. *J. Appl. Phys.* **93**, 2435–2439.

Papas, C. H. 1988 *Theory of electromagnetic wave propagation*. New York: Dover.

Ram-Mohan, L. R. 2002 *Finite element and boundary element applications in quantum mechanics*. Oxford University Press.

Rodin, G. J. 1996 Eshelby's inclusion problem for polygons and polyhedra. *J. Mech. Phys. Solids* **44**, 1977–1995.

Ru, C. Q. 2000 Eshelby's problem for two-dimensional piezoelectric inclusions of arbitrary shape. *Proc. R. Soc. Lond.* A **456**, 1051–1068.

Ru, C. Q. 2001 Two-dimensional Eshelby problem for two bonded piezoelectric half-planes. *Proc. R. Soc. Lond.* A **467**, 865–883.

Singh, J. 1993 *Physics of semiconductors and their heterostructures*. New York: McGraw-Hill.

Tiersten, H. F. 1969 *Linear piezoelectric plate vibrations*. New York: Plenum.

Ting, T. C. T. 1996 *Anisotropic elasticity*. Oxford University Press.

Volakis, J. L., Chatterjee, A. & Kempel, L. C. 1998 *Finite element method for electromagnetics*. New York: IEEE Press.

Waltereit, P., Romanov, A. E. & Speck, J. S. 2002 Electronic properties of GaN induced by a subsurface stressor. *Appl. Phys. Lett.* **81**, 4754–4756.

Willis, J. R. 1981 Variational and related methods for the overall properties of composites. *Adv. Appl. Mech.* **21**, 1–78.

Yu, H. Y. 2001 Two-dimensional elastic defects in orthotropic bicrystals. *J. Mech. Phys. Solids* **49**, 261–287.

Yu, H. Y., Sanday, S. C. & Chang, C. I. 1994 Elastic inclusion and inhomogeneities in transversely isotropic solids. *Proc. R. Soc. Lond.* A **444**, 239–252.